Research Article Vol. 58, No. 36 / 20 December 2019 / Applied Optics 9803

applied optics

# Multimode-fiber-coupled superconducting nanowire single-photon detectors with high detection efficiency and time resolution

Jin Chang,[1,*] Iman Esmaeil Zadeh,[1] Johannes W. N. Los,[2] Julien Zichi,[3] Andreas Fognini,[2] Monique Gevers,[2] Sander Dorenbos,[2] Silvania F. Pereira,[1] Paul Urbach,[1] and Val Zwiller[3]

[1]Optics Research Group, ImPhys Department, Faculty of Applied Sciences, Delft University of Technology, Lorentzweg 1, 2628 CJ Delft, The Netherlands
[2]Single Quantum B.V., 2628 CH Delft, The Netherlands
[3]Department of Applied Physics, Royal Institute of Technology (KTH), SE-106 91 Stockholm, Sweden
*Corresponding author: j.chang-1@tudelft.nl

Received 3 October 2019; revised 12 November 2019; accepted 12 November 2019; posted 13 November 2019 (Doc. ID 379683); published 11 December 2019

**In the past decade, superconducting nanowire single-photon detectors (SNSPDs) have gradually become an indispensable part of any demanding quantum optics experiment. Until now, most SNSPDs have been coupled to single-mode fibers. SNSPDs coupled to multimode fibers have shown promising efficiencies but have yet to achieve high time resolution. For a number of applications ranging from quantum nano-photonics to bio-optics, high efficiency and high time resolution are desired at the same time. In this paper, we demonstrate the role of polarization on the efficiency of multimode-fiber-coupled detectors and fabricated high-performance 20 μm, 25 μm, and 50 μm diameter detectors targeted for visible, near-infrared, and telecom wavelengths. A custom-built setup was used to simulate realistic experiments with randomized modes in the fiber. We achieved over 80% system efficiency and <20 ps timing jitter for 20 μm SNSPDs. Also, we realized 70% system efficiency and <20 ps timing jitter for 50 μm SNSPDs. The high-efficiency multimode-fiber-coupled SNSPDs with unparalleled time resolution will benefit various quantum optics experiments and applications in the future.** 

https://doi.org/10.1364/AO.58.009803 

## 1. INTRODUCTION

Generating and detecting light at the single-photon level has enabled a wide range of scientific breakthroughs in several fields, such as quantum optics, bio-imaging, and astronomy. High-performance single-photon sources have been realized in several platforms such as nonlinear crystals [1], color centers [2], atoms [3], molecules [4], and quantum dots (QDs) [5]. Collecting light from most of these single-photon emitters, however, is a challenge. For example, QDs have emerged as excellent sources of single photons with outstanding single-photon purity [6] and promising candidates for high-throughput generation of entangled photons [7,8]. Currently, most high-performance QDs are realized on III-V semiconductor platforms. Due to the nature of their emission and also the high refractive indices of these materials, extracting photons and coupling them to single-mode (SM) fibers has been a major challenge. Many groups have explored processing III-V QDs to enhance the coupling to optical fibers [9–11]. However, coupling photons from QDs to SM fiber, which has a low numerical aperture (NA) and a small core diameter, imposes demanding constraints on the laboratory setup. Multimode (MM) fibers, on the other hand, offer larger core diameters as well as higher NA, and provide several optical modes that significantly relax the task of optical coupling. In the field of tissue imaging, photons rapidly get scattered. After a short distance in the tissue, on the order of 1 mm, the transmitted ballistic light is attenuated by about 10 orders of magnitude [12]. Therefore, most collected photons are scattered and diffused ones. These photons cannot be easily collected and supported by SM fibers; thus, a large core, high NA, and many modes are necessary. Similarly, in remote laser ranging applications, e.g., a superconducting nanowire single-photon detector (SNSPD)-based lidar system, MM fibers are preferably chosen, since they offer a larger active area and easier coupling to telescopes compared with SM fibers. However, the SNSPDs used in the lidar system are smaller than the core size of MM fiber [13]. Thus, large-sized SNSPDs coupled to MM fiber with simultaneous high efficiency and high time resolution will benefit remote laser ranging applications.

Once light is coupled to fibers, SNSPDs are outstanding single-photon detectors because of their combined performances of high detection efficiency, high time resolution, and low dark count rate [14]. Attempts have been made to couple SNSPDs to 50 μm and 100 μm MM fibers [15–17]. Also, using lenses to focus the input beam, MM fibers were coupled to smaller SNSPDs and SNSPD arrays [18–20], but the achieved time resolution of the larger detectors have been limited to 76–105 ps. Recent works [21,22] suggested significant tradeoff between the SNSPD's length and its time response due to the geometrical jitter. However, a number of experimental observations [14,23–25] contradict this. Here, we also demonstrate a very high time resolution for large-area (long) SNSPDs.

In this paper, we design and fabricate SNSPDs for several wavelength bands spanning from visible (VIS) to telecom. To investigate the role of polarization on the system detection efficiency, we carefully characterized detectors using both standard SM fibers with polarization control and MM fibers with randomized modes and polarization. We also studied the influence of fiber dispersion on the instrument response function (IRF) of the system. Especially, with our low timing jitter 50 μm diameter SNSPD we extracted the jitter introduced by the geometrical factor. Compared to previous reports, the much lower timing jitter for large-sized SNSPDs in our work will benefit quantum optics experiments and applications in the future.

## 2. SNSPD FABRICATION AND MEASUREMENT SETUP

Similar to [14], we fabricated SNSPDs for the wavelength range of 500–1550 nm out of sputtered 9–11 nm thick films of NbTiN. Figure 1(a) shows a scanning electron microscopy image of two fabricated SNSPDS, where left and right images show SNSPDs with 20 μm and 50 μm diameters, respectively. To achieve saturation of internal efficiency, we fabricated the detectors for VIS and near infrared (NIR) using 10–11 nm films and the telecom SNSPDs out of 9 nm films. The meander width for VIS detectors was 100 nm, and for NIR and telecom, it was fixed to 70 nm. The filling factor in all cases was 0.5. As shown in Figs. 1(b) and 1(c), two optical setups were built to measure the system detection efficiency (SDE) of SNSPDs with SM and MM fibers. In Fig. 1(b), light from a laser diode is guided by SM fiber to a digital attenuator and polarization controller, and then coupled to another SM fiber that brings the light into the 2.4 K cryostat. The right of Fig. 1(b) shows the Gaussian mode of light inside the SM fiber. In order to evaluate the efficiency of MM coupled devices for practical applications, as shown in Fig. 1(c), light from a laser diode is coupled to an optical U-shape bench containing neutral density (ND) filters for attenuating the light power and two diffusers with different grades for generating hybrid light modes. Another MM fiber is used at the other end of the U-bench to couple light into the 2.4 K cryostat. Inside the cryostat, the same type of MM fiber is used to couple light to SNSPDs. As a comparison, the picture on the right side of Fig. 1(c) represents an image of the core of MM fiber at the output of the U-bench indicating hybrid modes in the 50 μm MM fiber.

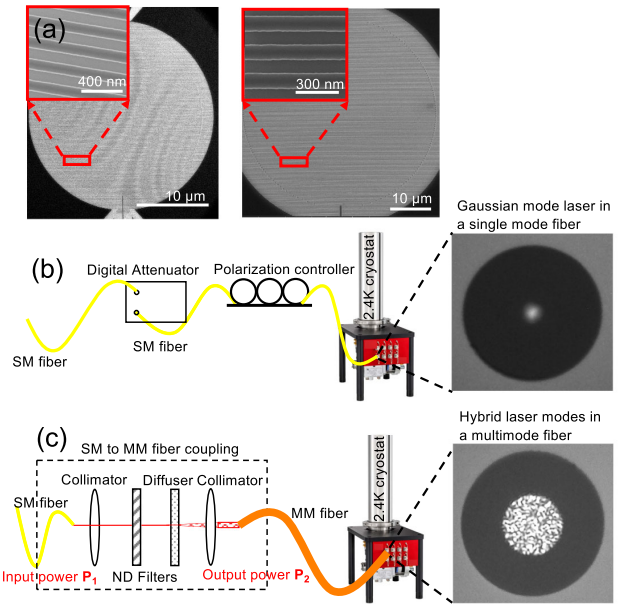


**Fig. 1.** (a) Scanning electron microscopy images of a 20 μm diameter SNSPD (left) and 50 μm diameter SNSPD (right). System detection efficiency measurement with two different setups: (b) SM fiber setup and (c) MM fiber setup.

## 3. SIMULATION AND SYSTEM DETECTION EFFICIENCY MEASUREMENT

Figure 2 shows the finite-difference time-domain (FDTD) simulation of three different optical cavities for enhancing the photon absorption in the meander. Since the absorption is dependent on the polarization of the vertically incident light [26], we simulated the maximum absorption (TE) and minimum absorption (TM) for Gaussian mode light. The average of TE and TM absorption, unpolarized (UP), is used to present the case where light is in hybrid mode. In Fig. 2(a), an aluminum mirror with a thin layer of $SiO_2$ (about 70 nm) is employed to enhance the absorption for a meander with 100 nm line width and 200 nm pitch. One benefit of this cavity is that the peak absorption wavelength can be simply shifted by tuning the thickness of the $SiO_2$ layer or adding extra $SiO_2$ on top. In Fig. 2(a), the absorption wavelength center is set around 525 nm. At 516 nm, the absorption of TE mode reaches 89%, while for the TM mode, it is 86%. As a result, the averaged absorption of TE and TM remains at about 87.5%. For 900 nm and 1550 nm, we simulated detectors on a distributed Bragg reflector (DBR) cavity for a better agreement with our experimental samples. In both cases, the DBR comprised 6.5 periods of $Nb_2O_5$ and $SiO_2$ bilayers. The thickness of $Nb_2O_5/SiO_2$ was 155/99 nm for 900 nm and 268/173 nm for 1550 nm. For both cases, we set the meander to be 70 nm line width and 140 nm pitch, which was the same in our fabrication process. In Fig. 2(b), the absorption of the TE mode approaches 92%, while TM mode is 52% at 900 nm, and the averaged value is 72%. At 1550 nm, the simulated TE and TM efficiencies, shown in Fig. 2(c), are 92% and 22%, respectively, which yields an average of 57%. This significant difference in absorption for TE and TM is due to stronger polarization dependence at telecom wavelength compared to VIS and NIR.

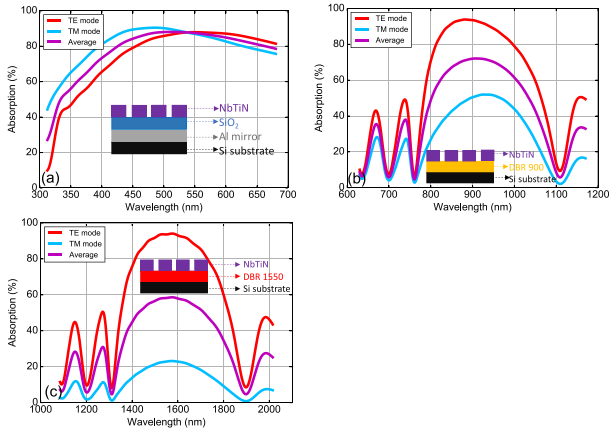


**Fig. 2.** Simulated reflectivity of (a) Aluminum/$SiO_2$ cavity for visible wavelength, (b) DBR for 900 nm, and (c) DBR for 1550 nm wavelength.

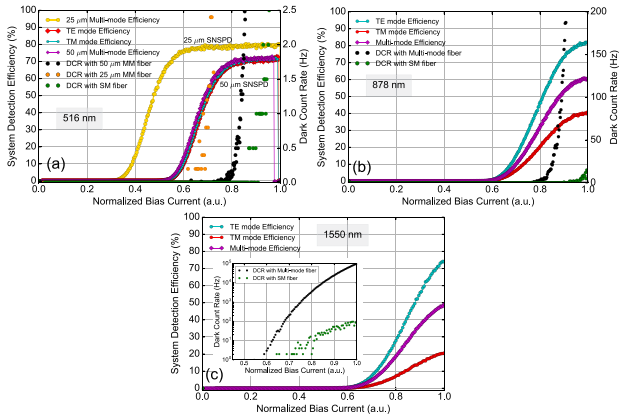


**Fig. 3.** (a) SDE of 25/50 μm diameter SNSPD at 516 nm, (b) SDE of a 20 μm diameter SNSPD at 878 nm, and (c) SDE of a 20 μm diameter SNSPD at 1550 nm.

To characterize SM SDE of our fabricated detectors, laser diodes with different wavelengths were used as photon sources (continuous wave). The power of the laser was recorded by a calibrated power meter and stabilized at 10 nW. After the power stabilization, an attenuation of BB was added by the digital attenuator, and then the laser was coupled to the SNSPD. For SDE measurement with MM fiber, we recorded the laser power before ($P_1$) and after ($P_2$) the U-bench with a calibrated power meter. By adding different ND filters in the U-bench, we controlled the ratio of $P_1/P_2$ close to 50 dB. Then we set the power of the input laser also at 10 nW for efficiency measurements. In both cases, the total input photon number can be back calculated from the input laser power. A commercial SNSPD driver was used to control the bias current and read the count rate. In all SDE measurements, we subtracted dark counts from the total photon counts, and this was negligible for SM measurements and MM measurements at VIS and NIR. However, telecom detectors coupled to MM fiber detect a significant amount of fiber-coupled blackbody radiation. We also removed another 3.6% to account for the end-facet reflection of the fiber where we measured the input power [14]. As shown in Fig. 3(a), at 516 nm, the SDE of the 50 μm detector is 70% measured with both SM (red/cyan curve) and MM (purple curve) fiber. All detectors show well-saturated internal efficiency. With SM fiber coupled to the SNSPD, there was negligible polarization dependence, which means the TE and TM modes are equally absorbed by the nanowire, and therefore, we also measured a similar efficiency with MM-fiber-coupled detectors. To avoid detector latching, we used a resistive bridge similar to [14]. We also fabricated 25 μm diameter SNSPDs (70 nm width/140 nm pitch) for VIS wavelength range. Since this detector was significantly larger than the fiber, it offers more alignment tolerance and better absorption of cladding modes. An SDE of about 80% was achieved for this type of detector coupled to a 20 μm fiber [yellow curve in Fig. 3(a)]. We also show dark count rates of SNSPDs with both SM fiber, 25 μm, and 50 μm MM fiber in Fig. 3(a). When SNSPDs reach saturated detection efficiency, the dark count rate is below 0.2 Hz for both SM and MM fiber coupling at 516 nm; however, for 878 nm, Fig. 3(b), and 1550 nm, Fig. 3(c), dark count rates are much higher when SNSPDs are coupled to MM fibers. As shown in the inset in Fig. 3(c), when 1550 nm SNSPD is coupled to MM fiber, the dark count rate is approximately 1000 times higher than the SM fiber coupling. This is caused by blackbody radiation coupled to fiber modes and detected by an efficient (compared to VIS and NIR) telecom detector.

At 878 nm as shown in Fig. 3(b), TE and TM mode detection efficiencies are significantly different. For optimized polarization (TE), the SDE approached 80%, while for TM polarization, SDE was only 40%. The polarization dependence ratio was a factor of two, which is in close agreement with our simulations. With our MM efficiency measurement setup, we coupled hybrid modes and fully illuminated the SNSPD. We measured an SDE of 60% for the MM-fiber-coupled detector at 878 nm, which is in perfect agreement with an average of TE and TM efficiencies measured with SM fiber. Similarly, at 1550 nm, the TE efficiency was 75% and TM was 20%. The measured polarization dependence was larger, a factor of 3.75, and thus the efficiency measured with MM fiber was only 50%. Polarization dependence can be improved by using index-matching top dielectric layers [27,28] at the cost of bandwidth or employing fractal structure detectors [29].

## 4. JITTER MEASUREMENT AND ANALYSIS

For SNSPDs, the IRF usually has a Gaussian distribution, and FWHM is commonly used as a value of IRF of the system, also known as jitter. In this work, we used a 50 MHz picosecond pulsed laser (4.2 ps pulse width) at 1064 nm and attenuated it to have much less than one photon per pulse (on detector $<50-100$ kHz count rate). The electrical reference signal was provided by a fast photo diode. An oscilloscope with 4 GHz bandwidth and 40 GHz sampling rate was used to record the SNSPD signal pulse and to measure the jitter. We triggered on the rising edge of the SNSPD pulse as the start signal, and triggered the same way on the synchronized electric reference signal as the stop. By building the distribution of time delay between start and stop, we acquired the IRF histogram and extracted its FWHM as jitter. In each jitter measurement, we recorded over 100,000 data points.

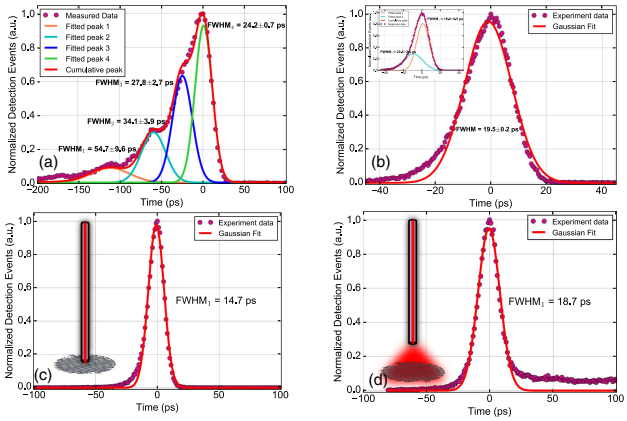


**Fig. 4.** Jitter measurement of (a) 20 μm diameter SNSPD with step-index MM fiber/room-temperature amplifier, (b) 20 μm diameter SNSPD with graded-index MM fiber/cryogenic amplifier, (c) 50 μm diameter SNSPD with SM fiber plugged tightly/cryogenic amplifier, and (d) 50 μm diameter SNSPD with SM fiber unplugged from detector/cryogenic amplifier.

As shown in Fig. 4(a), we measured the jitter of the above-mentioned 20 μm detector with 20 μm step-index MM fiber and room-temperature amplifier. Since different modes travel at different speeds in the step-index fiber, known as dispersion, many other peaks appear. By multi-peak fitting, we acquired the FWHM of each peak. From left to right, they are $54.7 \pm 9.6$ ps, $34.1 \pm 3.9$ ps, $23.8 \pm 2.7$ ps, and $24.2 \pm 0.7$ ps. The fitted peak 4 with highest FWHM ($24.2 \pm 0.7$ ps) is close to the jitter measured with SM fiber ($23.7 \pm 0.08$ ps). To overcome the fiber dispersion issue, we employed MM graded-index fiber (GIF), and to reduce noise-induced jitter, we used a cryogenic amplifier mounted at 40 K stage. As shown in Fig. 4(b), the red curve represents the Gaussian fitting function, and it gives a jitter of $19.5 \pm 0.2$ ps. This shows that graded-index MM fiber is the preferred choice for coupling to large-diameter detectors. It is worth mentioning that a noticeably asymmetric Gaussian shape of the histogram in Fig. 4(b) is observed, and in the inset, we show a two-peak fitting. According to a previous study [22], the main peak arises from the deterministic regime where jitter is controlled by a position-dependent detection threshold in straight parts of meanders. The lower side peak is caused in the probabilistic regime where the detector bends contribute. Our large-diameter SNSPDs also offer the opportunity to study geometrical jitter. As shown in Fig. 4(c), we first measured the jitter of a fabricated 50 μm SNSPD tightly connected to a SM fiber with a 5 μm mode field diameter and NA of 0.13. The measured timing jitter is 14.7 ps. Then in Fig. 4(d), we show jitter is 18.7 ps when the fiber is 4 mm away from the detector, which means the whole detection area is fully illuminated (calculated laser spot diameter is over 1 mm). Since the above two jitter measurements were carried out under exactly the same conditions, we extracted the difference in between:

$$\sqrt{b^2 - a^2} = 11.5 \text{ (ps)}. \quad (1)$$

This 11.5 ps consists of geometrical jitter and inhomogeneity-induced jitter [30]; however, the geometrical-factor-induced jitter is no more than 11.5 ps, which is two orders of magnitude lower than previously reported results [21,22]. (The total length of our 50 μm SNSPD is about 5 mm). The achieved jitter for both 20 μm and 50 μm SNSPDs in this work is the best reported time resolution for MM-fiber-coupled SNSPDs so far and will offer opportunities for future quantum optics experiments with high time resolution requirements.

## 5. CONCLUSION

In this paper, we designed, fabricated, and characterized MM-fiber-coupled SNSPDs for VIS, NIR, and telecom wavelengths. For VIS wavelength, polarization dependence was negligible; thus, both SM- and MM-coupled SNSPDs showed >80% system detection efficiency. For NIR and telecom wavelengths, polarization dependence plays an important role, and its ratio increases with wavelength. We reached 60% and 50% system detection efficiency with randomized mode illumination for 878 nm and 1550 nm, respectively. For jitter measurements, step-index MM fibers introduce light dispersion; thus, the IRF showed multiple peaks. By using graded-index MM fibers, this issue can be solved, and together with cryogenic amplifier readout circuitry, the jitter of MM-fiber-coupled SNSPDs can be improved to sub-20 ps. Since our MM-fiber-coupled SNSPDs have high system detection efficiency and high timing resolution at the same time, they can improve the performance of existing experiments in quantum optics, life sciences, and satellite-based space communication in the future.

**Funding.** China Scholarship Council (201603170247); Nederlandse Organisatie voor Wetenschappelijk Onderzoek (680-91-202); EC Horizon 2020 Framework Programme ATTRACT (777222).

**Disclosures.** The authors declare no conflicts of interest.

## REFERENCES

1. P. G. Kwiat, K. Mattle, H. Weinfurter, A. Zeilinger, A. V. Sergienko, and Y. Shih, "New high-intensity source of polarization-entangled photon pairs," Phys. Rev. Lett. **75**, 4337–4341 (1995).
2. C. Kurtsiefer, S. Mayer, P. Zarda, and H. Weinfurter, "Stable solid-state source of single photons," Phys. Rev. Lett. **85**, 290–293 (2000).
3. M. Saffman and T. Walker, "Creating single-atom and single-photon sources from entangled atomic ensembles," Phys. Rev. A **66**, 065403 (2002).
4. B. Lounis and W. E. Moerner, "Single photons on demand from a single molecule at room temperature," Nature **407**, 491 (2000).
5. M. E. Reimer, G. Bulgarini, N. Akopian, M. Hocevar, M. B. Bavinck, M. A. Verheijen, E. P. Bakkers, L. P. Kouwenhoven, and V. Zwiller, "Bright single-photon sources in bottom-up tailored nanowires," Nat. Commun. **3**, 737 (2012).
6. L. Schweickert, K. D. Jöns, K. D. Zeuner, S. F. Covre da Silva, H. Huang, T. Lettner, M. Reindl, J. Zichi, R. Trotta, A. Rastelli, and V. Zwiller, "On-demand generation of background-free single photons from a solid-state source," Appl. Phys. Lett. **112**, 093106 (2018).
7. N. Akopian, N. Lindner, E. Poem, Y. Berlatzky, J. Avron, D. Gershoni, B. Gerardot, and P. Petroff, "Entangled photon pairs from semiconductor quantum dots," Phys. Rev. Lett. **96**, 130501 (2006).
8. Y. Chen, J. Zhang, M. Zopf, K. Jung, Y. Zhang, R. Keil, F. Ding, and O. G. Schmidt, "Wavelength-tunable entangled photons from silicon-integrated iii-v quantum dots," Nat. Commun. **7**, 10387 (2016).

9. M. Pelton, C. Santori, J. Vučković, B. Zhang, G. S. Solomon, J. Plant, and Y. Yamamoto, "Efficient source of single photons: a single quantum dot in a micropost microcavity," Phys. Rev. Lett. **89**, 233602 (2002).
10. P. Schnauber, A. Thoma, C. V. Heine, A. Schlehahn, L. Gantz, M. Gschrey, R. Schmidt, C. Hopfmann, B. Wohlfeil, J.-H. Schulze, A. Strittmatter, T. Heindel, S. Rodt, U. Woggon, D. Gershoni, and S. Reitzenstein, "Bright single-photon sources based on anti-reflection coated deterministic quantum dot microlenses," Technologies **4**, 1 (2016).
11. X. Ding, Y. He, Z.-C. Duan, N. Gregersen, M.-C. Chen, S. Unsleber, S. Maier, C. Schneider, M. Kamp, S. Höfling, C.-Y. Lu, and J.-W. Pan, "On-demand single photons with high extraction efficiency and near-unity indistinguishability from a resonantly driven quantum dot in a micropillar," Phys. Rev. Lett. **116**, 020401 (2016).
12. J. A. Moon, R. Mahon, M. D. Duncan, and J. Reintjes, "Resolution limits for imaging through turbid media with diffuse light," Opt. Lett. **18**, 1591–1593 (1993).
13. J. Zhu, Y. Chen, L. Zhang, X. Jia, Z. Feng, G. Wu, X. Yan, J. Zhai, Y. Wu, Q. Chen, and X. Zhou, "Demonstration of measuring sea fog with an SNSPD-based lidar system," Sci. Rep. **7**, 15113 (2017).
14. I. E. Zadeh, J. W. Los, R. B. Gourgues, V. Steinmetz, G. Bulgarini, S. M. Dobrovolskiy, V. Zwiller, and S. N. Dorenbos, "Single-photon detectors combining high efficiency, high detection rates, and ultra-high timing resolution," APL Photon. **2**, 111301 (2017).
15. D. Liu, S. Miki, T. Yamashita, L. You, Z. Wang, and H. Terai, "Multimode fiber-coupled superconducting nanowire single-photon detector with 70% system efficiency at visible wavelength," Opt. Express **22**, 21167–21174 (2014).
16. H. Li, L. Zhang, L. You, X. Yang, W. Zhang, X. Liu, S. Chen, Z. Wang, and X. Xie, "Large-sensitive-area superconducting nanowire single-photon detector at 850 nm with high detection efficiency," Opt. Express **23**, 17301–17308 (2015).
17. C. Lv, H. Zhou, H. Li, L. You, X. Liu, Y. Wang, W. Zhang, S. Chen, Z. Wang, and X. Xie, "Large active area superconducting single-nanowire photon detector with a 100 μm diameter," Supercond. Sci. Technol. **30**, 115018 (2017).
18. L. Zhang, M. Gu, T. Jia, R. Xu, C. Wan, L. Kang, J. Chen, and P. Wu, "Multimode fiber coupled superconductor nanowire single-photon detector," IEEE Photon. J. **6**, 6802608 (2014).
19. L. Zhang, C. Wan, M. Gu, R. Xu, S. Zhang, L. Kang, J. Chen, and P. Wu, "Dual-lens beam compression for optical coupling in superconducting nanowire single-photon detectors," Sci. Bull. **60**(16), 1434–1438 (2015).
20. Q. Chen, B. Zhang, L. Zhang, R. Ge, R. Xu, Y. Wu, X. Tu, X. Jia, L. Kang, J. Chen, and P. Wu, "A 16-pixel NBN nanowire single photon detector coupled with 300 micrometer fiber," arXiv:1811.09779 (2018).
21. N. Calandri, Q.-Y. Zhao, D. Zhu, A. Dane, and K. K. Berggren, "Superconducting nanowire detector jitter limited by detector geometry," Appl. Phys. Lett. **109**, 152601 (2016).
22. M. Sidorova, A. Semenov, H.-W. Hübers, I. Charaev, A. Kuzmin, S. Doerner, and M. Siegel, "Physical mechanisms of timing jitter in photon detection by current-carrying superconducting nanowires," Phys. Rev. B **96**, 184504 (2017).
23. J. Wu, L. You, S. Chen, H. Li, Y. He, C. Lv, Z. Wang, and X. Xie, "Improving the timing jitter of a superconducting nanowire single-photon detection system," Appl. Opt. **56**, 2195–2200 (2017).
24. I. E. Zadeh, J. W. Los, R. Gourgues, G. Bulgarini, S. M. Dobrovolskiy, V. Zwiller, and S. N. Dorenbos, "A single-photon detector with high efficiency and sub-10 ps time resolution," arXiv:1801.06574 (2018).
25. H. Wang, H. Li, L. You, P. Hu, X. Zhang, W. Yong, W. Zhang, X. Yang, L. Zhang, H. Zhou, and Z. Wang, "Large-area multispectral superconducting nanowire single-photon detector," Appl. Opt. **58**, 8148–8152 (2019).
26. S. N. Dorenbos, E. M. Reiger, N. Akopian, U. Perinetti, V. Zwiller, T. Zijlstra, and T. M. Klapwijk, "Superconducting single photon detectors with minimized polarization dependence," Appl. Phys. Lett. **93**, 161102 (2008).
27. A. Mukhtarova, L. Redaelli, D. Hazra, H. Machhadani, S. Lequien, M. Hofheinz, J.-L. Thomassin, F. Gustavo, J. Zichi, V. Zwiller, and E. Monroy, "Polarization-insensitive fiber-coupled superconducting-nanowire single photon detector using a high-index dielectric capping layer," Opt. Express **26**, 17697–17704 (2018).
28. L. Redaelli, V. Zwiller, E. Monroy, and J. Gérard, "Design of polarization-insensitive superconducting single photon detectors with high-index dielectrics," Supercond. Sci. Technol. **30**, 035005 (2017).
29. X. Chi, K. Zou, C. Gu, J. Zichi, Y. Cheng, N. Hu, X. Lan, S. Chen, Z. Lin, V. Zwiller, and X. Hu, "Fractal superconducting nanowire single-photon detectors with reduced polarization sensitivity," Opt. Lett. **43**, 5017–5020 (2018).
30. Y. Cheng, C. Gu, and X. Hu, "Inhomogeneity-induced timing jitter of superconducting nanowire single-photon detectors," Appl. Phys. Lett. **111**, 062604 (2017).